

Diffusive regimes in a two-dimensional chiral fluid

Francisco Vega Reyes ^{1,2}, Miguel A. López-Castaño¹ & Álvaro Rodríguez-Rivas ³✉

Diffusion is a fundamental aspect of transport processes in biological systems, and thus, in the development of life itself. And yet, the diffusive dynamics of active fluids with directed rotation, known as chiral fluids, has not been analyzed in detail so far. Here, we describe the diffusive regimes of a two-dimensional chiral fluid, composed in this case of a set of identical disk-shaped rotors. We found strong experimental evidence of odd diffusion. This odd diffusion emerges in the form of a two-dimensional tensor with an antisymmetric part. In particular, we show that chiral diffusion is complex, featuring transitions between super, quasi-normal, and sub diffusion, and very slowly aging. Moreover, we show that the diffusion tensor elements, including off-diagonal elements; i.e., odd diffusion coefficient, change sign according to flow vorticity. Therefore, the chiral fluid has a self regulated diffusion, controlled by its vorticity.

¹Departamento de Física, Universidad de Extremadura, 06071 Badajoz, Spain. ²Instituto de Computación Científica Avanzada (ICCAEx), Universidad de Extremadura, 06071 Badajoz, Spain. ³Department of Physical, Chemical and Natural Systems, Pablo de Olavide University, 41013 Sevilla, Spain.
✉email: arodriguezrivas@upo.es

Chiral fluids display a rather complex dynamics, featuring a variety of peculiar properties that cannot be found in traditional fluids. Albeit these properties actually play a major role in biological processes¹, where flow chirality is ubiquitous², research work on this line is currently in progress^{3–8}. In fact, the hydrodynamics of chiral fluids is characterized by an antisymmetric component in the stress tensor, and by a whole new set of transport coefficients. These new coefficients, allusively dubbed as odd (due to their chiral origin⁹) include new contributions (for instance, to viscosity^{9–11}). Diffusion is illustrative in that, whereas it has been extensively studied in a variety of materials since long ago^{12–15}, the development of diffusion theory for chiral fluids is relatively recent¹⁶. For instance, no experimental evidence of odd diffusion in a chiral fluid of active rotors has been provided so far (although there are experimental evidences in colloids under magnetic fields)^{17–20}. Furthermore, in the present work, we provide strong experimental evidence of a rich and complex diffusive behavior.

Parity and time reversal symmetry break imply the emergence of particle velocity cross correlations²¹, which necessarily yields, as we will see, an asymmetric diffusion tensor

$$\mathcal{D} = \begin{bmatrix} D & -D^{\text{odd}} \\ D^{\text{odd}} & D \end{bmatrix}, \quad (1)$$

where each of the two coefficients appearing in (1), including those corresponding to the antisymmetric component of \mathcal{D} , D^{odd} , can be calculated according to the Green-Kubo^{16,22–24} relations

$$D = \frac{1}{2} \int_0^\infty dt \langle v_i(t) v_j(0) \delta_{ij} \rangle, \quad (2)$$

$$D^{\text{odd}} = -\frac{1}{2} \int_0^\infty dt \langle v_i(t) v_j(0) \epsilon_{ij} \rangle, \quad (3)$$

with δ_{ij} , ϵ_{ij} being the Kronecker delta and the 2D Levi-Civita symbol, respectively. In eq. (2), diagonal elements (D) represent the Brownian diffusion coefficient, whereas off-diagonal elements (D^{odd}) stand for what we denoted as odd diffusion coefficient, in close analogy with odd viscosity⁹.

A recent theoretical model has predicted a diffusion tensor of the form in Eq. (1) as well¹⁶. However, in this model, the sign of D^{odd} is enslaved to the sign of particle activity. By contrast, we show now that chiral diffusion is governed, at the experimental level, by chiral flow vorticity (thus, by a fluid property, not a particle property). Furthermore, we describe a peculiar diffusive behavior. Beyond the question of the existence of the odd diffusion coefficient D^{odd} , we also found that: (i) chiral diffusion is always very slowly aging, and (ii) the chiral fluid is in general super-diffusive but can decay to normal diffusion or sub-diffusive behavior, with these transitions being controlled by flow vorticity as well.

Results

Description of the system. We performed experiments with a prototypical chiral fluid system. Here, the fluid consists of a set of identical disks-shaped particles. The disk diameter is $\sigma = 7.25$ cm, mass is $m_p = 7.1$ g, and $I \simeq (1/8)m_p \sigma^2 = 46$ g cm² is the moment of inertia. Each particle features a set of 14 evenly spaced, equally tilted blades. This geometrical configuration yields an intrinsic rotational chirality to the particles, which results in stationary chiral flows²¹. The disks translations are driven by turbulent air wakes produced by a homogeneous air upflow past the particles (for a more complete description of the driving mechanism, see ref. 21). This upflow also generates a continuous disk spin, as it goes through the blades. Due to their blade tilt angle, our particles spin clockwise (i.e., negative spin, according to mathematical

convention). The disks are confined within a horizontal circular region of diameter $L = 72.5$ cm. Each experiment is recorded for 100 s with a high-speed video camera. From experiments movies we obtain, by means of a particle tracking algorithm²⁵, the data presented in this work. See the Methods section for more details on the experimental methods.

Our analysis will be based on the spatial average of the fluid vorticity, $\bar{\omega}$. Here, we define flow vorticity as $\omega = (1/2)\epsilon_{ij}\partial_i u_j$. (As we will later see, $\bar{\omega}$ controls the diffusive behavior.) It is also convenient to define the packing fraction as $\phi \equiv N(\sigma/L)^2$, where N is the number of rotors present in the system (in our sets of measurements, $3 < N < 70$).

Mean squared and cross displacements. In Fig. 1 we analyze the properties of the averages of particle displacements. In particular, Fig. 1a shows the ensemble mean squared displacement $\langle \Delta r(t)^2 \rangle \equiv \langle \Delta x(t)^2 + \Delta y(t)^2 \rangle$, where $\Delta x(t)^2 \equiv (1/\mathcal{N}(t)) \sum_{\{t_0\}} [x(t+t_0) - x(t_0)]^2$, for positive, negative and zero global vorticity. (Since we deal with steady states only, displacements can be obtained, for each lag time t , from an average over the $\mathcal{N}(t)$ available initial states t_0 .) In logarithmic scale, $\langle \Delta r(t)^2 \rangle$ grows until confinement effects enter into action (particles should display diffusive arrest at, approximately, half the system size²⁶). As we see, the slope (in logarithmic scale) of $\langle \Delta r(t)^2 \rangle$ remains slightly varying at all times; i.e., never behaves quite linearly enough, contrary to the linear behavior in normal diffusion²⁷. In this figure we represent two slopes ($\alpha = 1$, $\alpha = 2$), making it clear that the system is superdiffusive ($2 > \alpha > 1$). Furthermore, in most cases, the slope never reaches the typical value for normal diffusion, that is, $\alpha = 1$.

Figure 1b displays the corresponding time evolution of the ensemble mean cross displacement $\langle \Delta x(t)\Delta y(t) \rangle$. With $\Delta x(t)\Delta y(t) = (1/\mathcal{N}(t)) \sum_{\{t_0\}} [x(t+t_0) - x(t_0)][y(t+t_0) - y(t_0)]$. This ensemble average would in general be zero in a system without chirality, and for this reason is usually not measured²⁷. Here, however, $\langle \Delta x(t)\Delta y(t) \rangle \neq 0$ in general. Nevertheless, we observe that $\langle \Delta x(t)\Delta y(t) \rangle$ remains null during a significantly long time interval. Furthermore, for experiments with $\bar{\omega} \simeq 0$, $\langle \Delta x(t)\Delta y(t) \rangle$ is nearly null at all times. Otherwise, the mean cross displacement is monotonically increasing/decreasing for $\bar{\omega} > 0$, $\bar{\omega} < 0$ respectively. This property has been measured during a time shorter than one fluid complete revolution but, in any case, a wide range of values is observed within this interval. This provides rich information on the behavior in the relevant parameter space. The dynamics of particle displacements is shown for more clarity also in the Supplementary Movie 1.

Finally, in panel (c) of Fig. 1, we see a spiral-like behavior of $\langle \Delta r_i(t) v_j(0) \epsilon_{ij} \rangle$ vs. $\langle \Delta r_i(t) \Delta v_j(0) \delta_{ij} \rangle$, for $\bar{\omega} \neq 0$. The shape of these spirals indicate that, in effect, we observe strong odd diffusion in general, but with important departures from results reported previously in theoretical models^{16,17,28}. In effect, we notice that, to the best of our knowledge, a new feature appears here, in the form of a kink with reverse curvature that develops at early times, near the transitional region $\bar{\omega} \simeq 0$. As $\bar{\omega}$ decreases, this kink with reverse curvature becomes bigger, which results in a combination of two opposite curvature spirals. The kink eventually occupies the complete spiral which, by means of this continuous mechanism, reverses its curvature sign (we point out here that the typical measurement error is 100 times smaller than the size of the kink and thus this feature is captured here with a high level of accuracy). As we said, this observation suggests that the change of sign of the odd diffusion coefficients occurs gradually. Moreover, it appears to be mediated by a (to our knowledge) not previously reported behavior where the odd coefficient alternatively changes its sign as time evolves (i.e., in some chiral stationary flows, the sign of the odd diffusion is not clearly

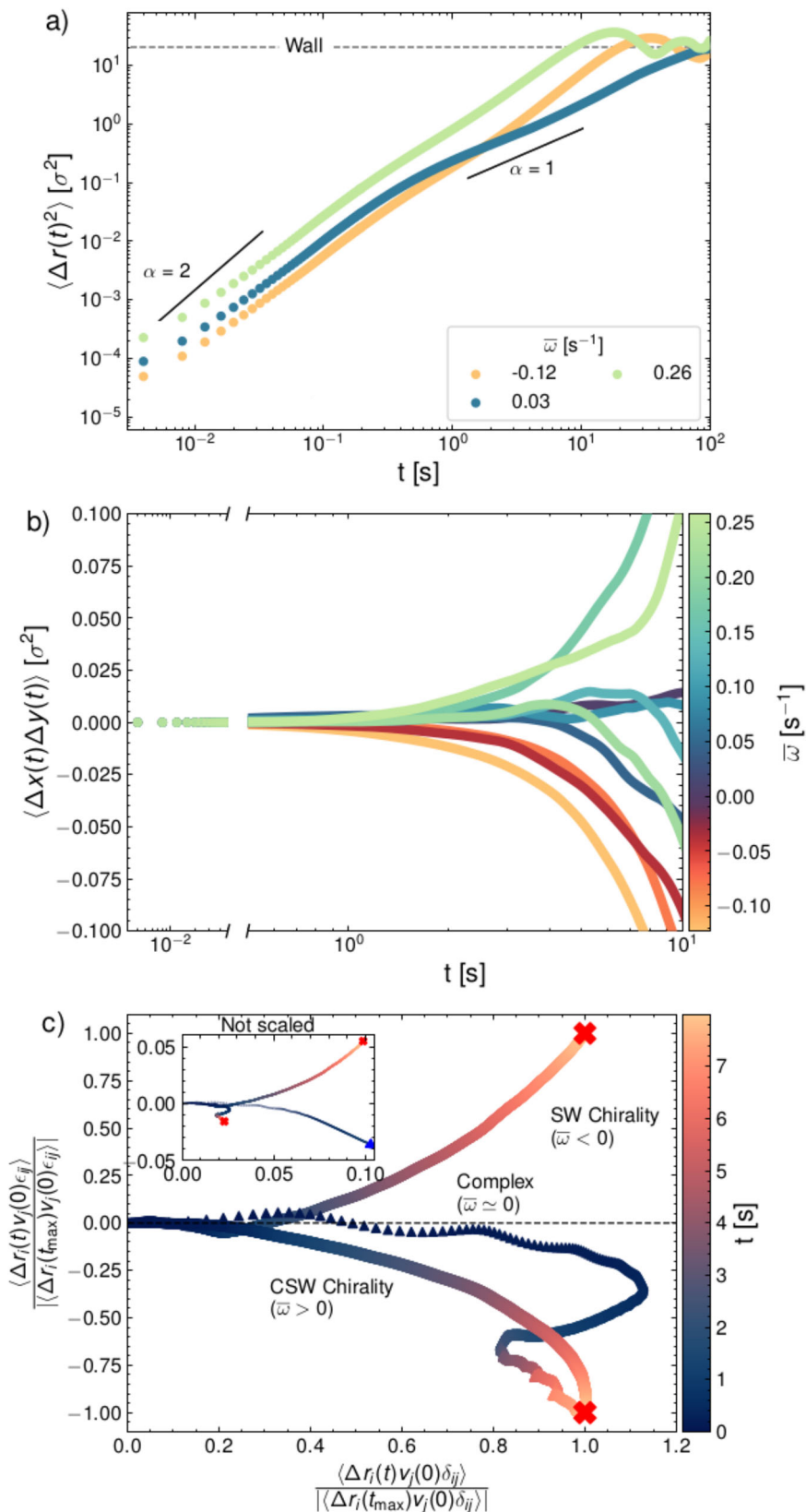


Fig. 1 Statistical properties of particle displacements. **a** Mean squared displacement $\langle \Delta r(t)^2 \rangle$ at three different global vorticities $\bar{\omega}$. The saturation value due to confinement is indicated with a dashed line. **b** Mean cross-displacements $\langle \Delta x(t)\Delta y(t) \rangle$ for several values of $\bar{\omega}$. **c** Position-velocity cross correlations for $\bar{\omega} = -0.12 \text{ s}^{-1}$, $\bar{\omega} = 0.03 \text{ s}^{-1}$, $\bar{\omega} = 0.26 \text{ s}^{-1}$ (indicated as $\bar{\omega} < 0$, $\bar{\omega} = 0$, $\bar{\omega} > 0$ respectively). In the main panel of **c**, correlations are scaled with the corresponding value at $t = t_{\max} = 8 \text{ s}$ (the last represented value in this case), while in inset shows the unscaled version. Packing fraction for **a-c**: $\phi = 0.45$.

defined). Supplementary Fig. 1 shows the transitions of the spiral curvatures and evolution of their kinks in more detail.

In order to provide also a description of the microscopic structure of diffusion, we represent in Fig. 2 the distribution functions of the root of the squared displacements, $\Delta r(t)$, reduced here with the standard deviation $\text{std}(\Delta r(t))$. We plot the results for a set of lag times, so that we can track eventual deviations off the Gaussian distribution (i.e., deviations from normal diffusion²⁷). We can detect strong deviations from normal diffusion for the $\bar{\omega} < 0$ (Fig. 2a) and $\bar{\omega} > 0$ (Fig. 2c) cases. Moreover, these deviations slowly vary as the system ages. Also, deviations from Gaussian behavior bifurcate for $\bar{\omega} < 0$ at longer lag times, see panel (a) (and also Supplementary Movie 1). On the contrary, $f(\Delta r/\text{std}(\Delta r))$ deviations from the Gaussian preserve the same structure at all times for $\bar{\omega} \simeq 0$ and they occur in the range of short displacements only, thus indicating that diffusion is less complex in this case. For more detail, see also Supplementary Fig. 2 for a three-dimensional representation of the excess kurtosis of $f(\Delta r/\text{std}(\Delta r))$. We found that that $f(\Delta r/\text{std}(\Delta r))$ is always platykurtic; i.e., the displacements distributions inherently have thinner tails. In addition, we have observed that the distribution function of cross displacements is clearly asymmetric when a strong chiral flow is present (i.e., when $|\bar{\omega}|$ is not small), which seems to indicate also that the chiral flow is the origin of odd diffusion in our system. See Supplementary Fig. 3 for details on the behavior of $f(\Delta x(t)\Delta y(t))$.

Diffusion coefficients. The results for the diffusion coefficients D, D^{odd} , as obtained from Eqs. (2), (3), are shown in Fig. 3. It is to be noticed that odd diffusion (right panel) is quite significant in most of the parameter space, since D^{odd} is close to the order of magnitude of D (left panel), except in the region of $\bar{\omega} \simeq 0$, where D^{odd} systematically falls to zero. Furthermore, Fig. 3 clearly reveals that $\bar{\omega} = 0$ signals in all cases the points where $D^{\text{odd}} = 0$ and the absolute minimum of D (and hence, the trend inversion of D). Moreover, all the curves for different densities collapse into one when represented against global vorticity, as an additional strong experimental evidence that, in effect, global vorticity $\bar{\omega}$ is the true control parameter for the diffusive regimes in a two-dimensional chiral fluid. This means that diffusion in the two-dimensional fluid is controlled by the global vorticity of the chiral flow; i.e., a fluid property, and not a microscopic property (such as particle activity/chirality^{16,17}). This can be best seen in the insets of Fig. 3, where the coefficients are also represented as a function of particle activity (here, the ensemble average spin, denoted as $\bar{\Omega}$). Furthermore, although the system is locally heterogeneous, we have observed that the sign of $\bar{\omega}$ is the same throughout the system²¹; i.e., the sign of chiral flow vorticity is a global property of the system (except for $\bar{\omega} \simeq 0$, where the behavior becomes more complex). This allows us for spatially averaging the diffusion tensor components, which aids to detect the relevant regimes in this kind of complex dynamics.

Results from Figs. 1a and 2 are actually revealing that mean square displacements for chiral fluids do not show in general (except, and only approximately, for the cases with $\bar{\omega} \simeq 0$) the typically exponential behavior of both normal and anomalous diffusion²⁷. In addition, it is also apparent that the slope of the corresponding curve $\langle \Delta r(t)^2 \rangle$ vs. t in log scale is time varying, as we said. This is in fact in close analogy with the behavior of jammed granular systems^{29,30} (indicates a varying exponential diffusion coefficient, as it happens in granular jamming²⁹).

In order to analyze this feature in more detail, we plot in Fig. 4 the time evolution of the diffusive exponent (α) of D , defined^{27,30} as $\langle \Delta r(t)^2 \rangle = (4D)t^\alpha$.

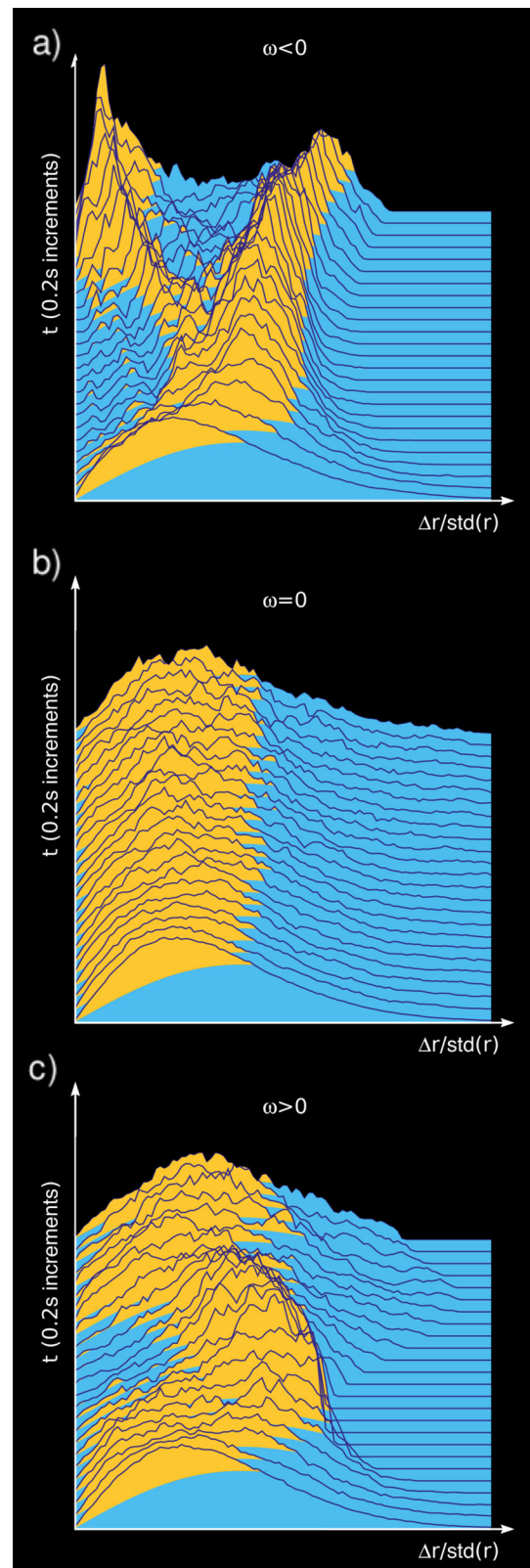


Fig. 2 Time evolution of the distribution function of the root of the reduced square displacements, $f(\Delta r/\text{std}(\Delta r))$. We display results for **a** $\bar{\omega} = -0.15 \text{ s}^{-1}$, **b** $\bar{\omega} = 0.08 \text{ s}^{-1}$ and **c** $\bar{\omega} = 0.23 \text{ s}^{-1}$ (indicated as $\bar{\omega} < 0$, $\bar{\omega} = 0$, $\bar{\omega} > 0$ respectively), with packing fraction $\phi = 0.45$. Being $\text{std}(\Delta r)$ the standard deviation of $\Delta \mathbf{r}$. In orange, the areas where $f(\Delta r/\text{std}(\Delta r)) > f_G$ and blue where $f(\Delta r/\text{std}(\Delta r)) < f_G$ (here, f_G is the normal Gaussian distribution).

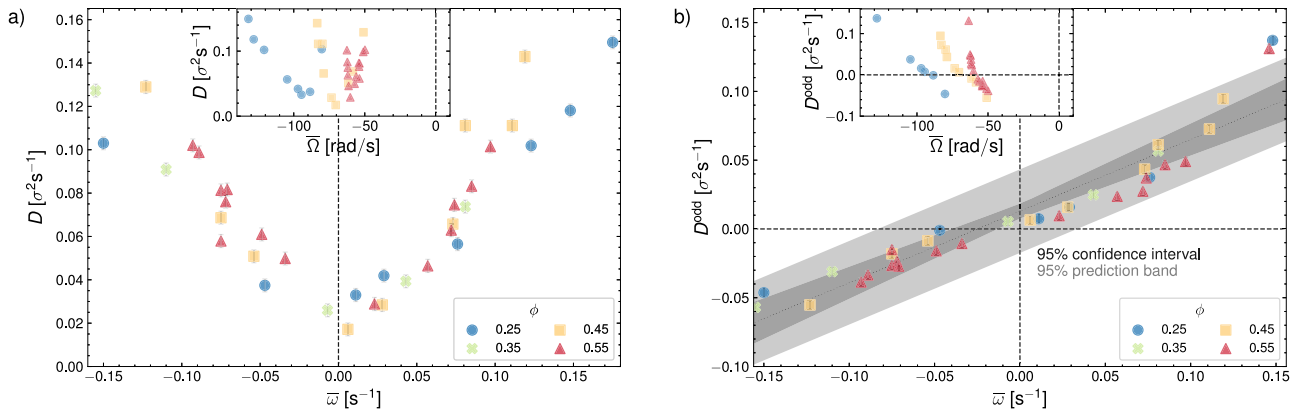


Fig. 3 Diffusion coefficients D , D^{odd} vs. global mean vorticity $\bar{\omega}$. Results are represented for several experiments at different densities (each denoted with a different symbol and color, see figure legend). **a** Diffusion coefficient D (diagonal elements of diffusion tensor \mathcal{D} , in eq. (1)). **b** Odd diffusion D^{odd} coefficient (off-diagonal elements of \mathcal{D}). Confidence intervals of a linear regression from the experimental data for D^{odd} appear shaded in gray. Insets display diffusion coefficients vs. particle activity (here, average particle spin $\bar{\Omega}$). Notice that in the insets D^{odd} changes sign at different points, contrary to the behavior with respect to the true control parameter $\bar{\omega}$ (main panels).

All three cases $\bar{\omega} < 0$, $\bar{\omega} \simeq 0$, $\bar{\omega} > 0$ undergo a slow decay off the initial ballistic regime ($\alpha = 2$) at short times (slow refers here at time intervals much longer in the diffusion curves than the ballistic regime, this is shorter than 0.01 s). Moreover, at high densities ($\phi = 0.45$, Fig. 4a), the case $\bar{\omega} \simeq 0$ has a diffusive exponent α that slowly decays to nearly normal diffusion ($\alpha = 1$). On the contrary, the other two cases ($\bar{\omega} \neq 0$) remain superdiffusive, with large oscillations around a mean value $\alpha \sim 1.5$ at high densities. Consequently, the inset of Fig. 4a reveals strong superdiffusion in a large fraction of the parameter space, in this case for a system with packing fraction $\phi = 0.45$. However, at low densities ($\phi = 0.25$, Fig. 4b) the phase behavior of diffusion seems to be qualitatively different. Now the system displays normal or weakly subdiffusive behavior for $\bar{\omega} \simeq 0$ and $\bar{\omega} > 0$ cases, whereas the $\bar{\omega} < 0$ case remains strongly superdiffusive (it would require to go to much larger densities in order to detect jamming or glassy behavior). In all cases, α sharply falls to $\alpha = 0$ at very long times, due to the effect of the wall confinement²⁷.

Discussion

In summary, we have provided an exhaustive description of the experimental behavior of chiral diffusion in a two-dimensional fluid of active particles. It is worth to remark that an odd diffusion coefficient D^{odd} is indeed experimentally measurable in chiral flows. However, and although D^{odd} is frequently as large as the usual diffusion coefficient D , our experiments reveal that odd diffusion can also be absent for active particles (i.e., at non-zero particle activity, see inset in Fig. 3b), contrary to what has been recently predicted¹⁶. Thus, more theoretical analysis should be performed on this important question.

Moreover, we find as well the following chiral diffusion regimes: (I) diffusion coefficient D is superdiffusive, accompanied with large odd diffusion coefficient D^{odd} (predominant regime); (II) diffusion coefficient is weakly subdiffusive, with large odd diffusion coefficient D^{odd} ; (III) the chiral fluid displays quasi-normal diffusion, with vanishing odd diffusion D^{odd} . For all three diffusive regimes, the diffusion coefficient D decays very slowly from ballistic to diffusive regime, which is prone to the emergence of memory effects³¹. Furthermore, in the few cases where the system becomes subdiffusive (Fig. 4b), the logarithmic slope of displacements changes continuously (Fig. 1a) and is not accompanied by a plateau, as it happens in molecular³² and granular glasses³⁰ (where subdiffusive particles are caged by the neighbors and only at long times, diffusing from a cage to the next); i.e. subdiffusion in chiral fluids appears to be rather peculiar with

respect to their analogs. It is important to highlight that a very recent study of the structure factor by means of simulation shows locally jammed states and multi-scale hyperuniformities for unconfined active spinners³³, which may be related to the weakly subdiffusive behavior that we observe here.

In addition, Fig. 1b shows that the time evolution of the mean cross displacement remains null for early to mid development stages, and emerging only (when it does) as the trajectories age enough, which results in a peculiar structure of the Brownian movement of the particles in the chiral fluid, as illustrated in Fig. 1 (and, more directly, in Supplementary Fig. 4).

Most importantly, we have discovered that the control parameter of chiral diffusion is the flow vorticity $\bar{\omega}$. This is supported by the strong and first (to the best of our knowledge) experimental evidence of the universal curves of the diffusion coefficients vs. $\bar{\omega}$ in Fig. 3. It actually makes sense that diffusion does not depend on (chiral) particle activity alone, since one could expect that the underlying chiral fluid flow has a strong impact on diffusion processes. In fact, this agrees very well with the recent experimental evidence that flow vorticity is not controlled by particle activity either²¹. Furthermore, the transitions between the aforementioned three diffusive regimes were still detected in spite of nearly constant reduced activity (see Supplementary Fig. 5, where insets of Fig. 3 are represented with more detail), which renders impossible that reduced particle activity can control chiral and hence odd diffusion.

This fundamental feature of odd diffusion in our system, and most of the other ones described in the present work, had not been reported previously and in fact they could not be trivially expected from a theoretical point of view. Our results are actually more reminiscent of more realistic biological systems with non-lattice (directionally) correlated random walks³⁴. It remains for future work the development of a theoretical framework that can account for the mechanisms causing these peculiar features of chiral diffusion in two dimensions in experimental systems. We are currently making progress in this sense.

In a broader context, the behaviors described here altogether draw a landscape of diffusion for two-dimensional chiral fluids that is very complex and peculiar, and probably unique in nature. We think this can potentially help to describe important dynamical processes in biologic systems.

Methods

In our experiments we use N identical 3D-printed disks (.stl models are available upon request), made of polylactic acid (PLA). Each disk has 14 equally spaced

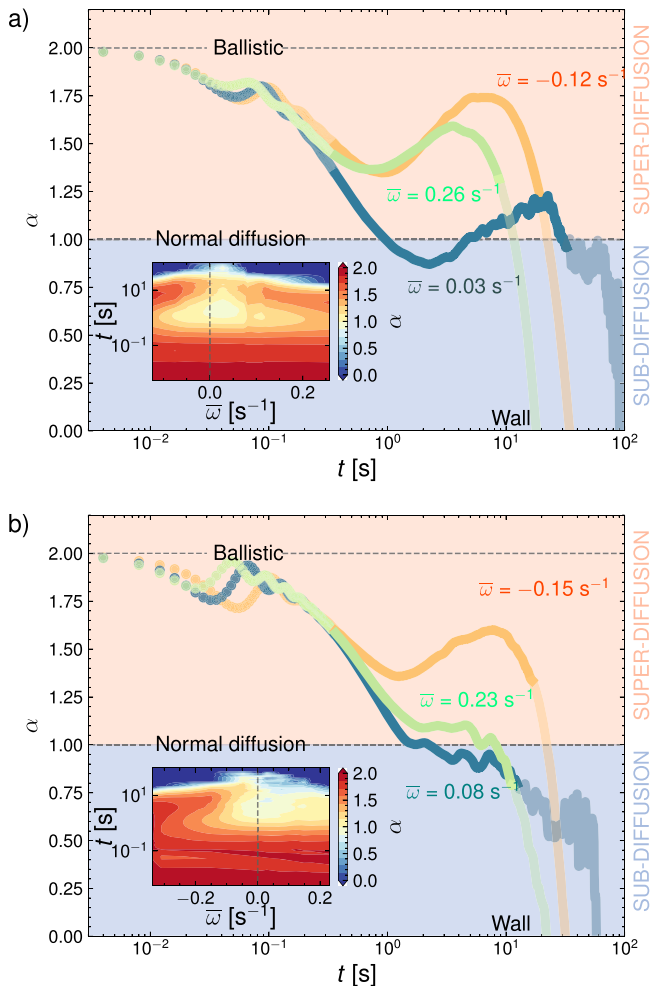


Fig. 4 Evolution of the diffusive exponent α . We show the results for three experiments with $\bar{\omega} < 0$, $\bar{\omega} = 0$, $\bar{\omega} > 0$ respectively (each represented in a different color of curve), at two different packing fractions: **a** $\phi = 0.45$ and **b** $\phi = 0.25$. Here, t represents lag time. The diffusive exponent has been calculated by performing a rolling fit of the mean squared displacement to a t^α slope. The ballistic regime and normal diffusion regimes are signaled with horizontal lines at $\alpha = 2$ and $\alpha = 1$, respectively. Translucent lines indicate that the system boundary has been reached. Heat-maps in the insets represent α in the $\bar{\omega} - t$ plane (notice the dip at large t , for the case $\bar{\omega} \simeq 0$).

identical oblique blades that generate a clock-wise spinning as upflow passes through the disk. Turbulent vortices from the upflow past the particles produces a stochastic translational motion as well. The rotors are located on top of a perforated steel sheet (3 mm diameter holes in a hexagonal pattern, with a 3 mm spacing). This metallic grid is mounted on a box that guides an adjustable air current, generated by a fan and homogenized by means of a polyurethane foam layer that is placed below the metallic grid. The upflow intensity is adjusted so that all particles levitate at the minimum possible height over the grid, thus avoiding friction. The air flow has been produced by a SODECA HCT-71-6T-0.7 fan, and its uniformity was verified with an anemometer. Local deviations of air flow caudal are found to be within $\pm 5\%$. Mean air flows ranged from 2.2 to 3.2 m/s. Particle movement is limited to a circular region with diameter $L = 725 \pm 1$ mm, located at the center of the metallic grid and delimited by walls of a height of 40 mm. We used a variable number of disks N ranging from 3 to 70 (equivalent here to packing fractions $\phi = 0.03$ to $\phi = 0.70$).

We have recorded a total of 120 experiments, varying the parameters (density and air current) and filmed with a Phantom VEO 410L high-speed camera. Each experiment movie contains a series of digital images at a rate of 250 fps, during 100 s. Our images achieve a spatial resolution of $\sim 0.05\%$ of the particle diameter. From each series of images (movie) we compute trajectories, vorticity and other whole-system properties. Trajectories are obtained by means of a modified version

of the algorithm by Crocker and Grier²⁵. The typical error for particle location is $\delta r \lesssim 0.1$ pixel, (which is near the inherent maximum accuracy in terms of pixels that can be obtained from the particle tracking method we used²⁵). A similar experimental configuration has been successfully employed recently in a series of experiments for studies on active particle dynamics^{35,36}.

Data availability

The data tables (particle positions and angles during experiments) that support the plots within this paper and other findings of this study are at the disposal of the reader and available in the following repository: <https://doi.org/10.5281/zenodo.6121454>.

Code availability

The exact version of the particle tracking codes that were used for this work are available in the following web link <https://doi.org/10.5281/zenodo.7226255>. Further updated versions will be available at <https://github.com/fvegar/blades>.

Received: 11 April 2022; Accepted: 30 September 2022;

Published online: 21 October 2022

References

1. Metzler, R., Jeon, J.-H. & Cherstvy, A. Non-brownian diffusion in lipid membranes: experiments and simulations. *Biochim. Biophys. Acta* **1858**, 2451 (2016).
2. Vicsek, T. & Zafeiris, A. Collective motion. *Phys. Rep.* **517**, 71 (2012).
3. Wu, Y., Hosu, B. G. & Berg, H. C. Microbubbles reveal chiral fluid flows in bacterial swarms. *Proc. Natl Acad. Sci. USA* **108**, 4147 (2011).
4. Petroff, A. P., Wu, X.-L. & Libchaber, A. Fast-moving bacteria self-organize into active two-dimensional crystals of rotating cells. *Phys. Rev. Lett.* **114**, 158102 (2015).
5. Belovs, M. & Cebers, A. Hydrodynamics with spin in bacterial suspensions. *Phys. Rev. E* **93**, 062404 (2016).
6. Wu, X.-L. & Libchaber, A. Particle diffusion in a quasi-two-dimensional bacterial bath. *Phys. Rev. Lett.* **84**, 3017 (2000).
7. Echeverria-Huarte, I., Nicolas, A., Cruz Hidalgo, R., Garcimartín, A. & Zuriguel, I. Spontaneous emergence of counterclockwise vortex motion in assemblies of pedestrians roaming within an enclosure. *Sci. Rep.* **12**, 2647 (2022).
8. Zhang, B., Yuan, H., Sokolov, A., de la Cruz, M. O. & Snezhko, A. Polar state reversal in active fluids. *Nat. Phys.* **18**, 154 (2022).
9. Avron, J. E. Odd viscosity. *J. Stat. Phys.* **92**, 543 (1998).
10. Banerjee, D., Souslov, A., Abanov, A. G. & Vitelli, V. Odd viscosity in chiral active fluids. *Nat. Commun.* **8**, 1573 (2017).
11. Han, M. et al. Fluctuating hydrodynamics of chiral active fluids. *Nat. Phys.* **17**, 1260 (2021).
12. Klett, K., Cherstvy, A. G., Shin, J., Sokolov, I. M. & Metzler, R. Non-gaussian, transiently anomalous, and ergodic self-diffusion of flexible dumbbells in crowded two-dimensional environments: coupled translational and rotational motions. *Phys. Rev. E* **104**, 064603 (2021).
13. Cuertos, A. & Patti, A. Dynamics of hard colloidal cuboids in nematic liquid crystals. *Phys. Rev. E* **101**, 052702 (2020).
14. Ghosh, S. K., Cherstvy, A. G., Grebenkov, D. S. & Metzler, R. Anomalous, non-gaussian tracer diffusion in crowded two-dimensional environments. *N. J. Phys.* **18**, 013027 (2016).
15. Kob, W. & Andersen, H. C. Scaling behavior in the β -relaxation regime of a supercooled lennard-jones mixture. *Phys. Rev. Lett.* **73**, 1376 (1994).
16. Hargus, C., Epstein, J. M. & Mandadapu, K. K. Odd diffusivity of chiral random motion. *Phys. Rev. Lett.* **127**, 178001 (2021).
17. van Teeffelen, S. & Löwen, H. Dynamics of a brownian circle swimmer. *Phys. Rev. E* **78**, 020101 (2008).
18. Zhang, B., Sokolov, A. & Snezhko, A. Reconfigurable emergent patterns in active chiral fluids. *Nat. Commun.* **11**, 4401 (2020).
19. Reeves, C. J., Aranson, I. S. & Vlahovska, P. M. Emergence of lanes and turbulent-like motion in active spinner fluid. *Commun. Phys.* **4**, 92 (2021).
20. Billign, E. S. et al. Motile dislocations knead odd crystals into whorls. *Nat. Phys.* **18**, 212 (2022).
21. López-Castaño, M. A., Márquez Seco, A., Márquez Seco, A., Rodríguez-Rivas, A. & Vega Reyes, F. Chirality transitions in a system of active flat spinners. *Phys. Rev. Res.* **4**, 033230 (2022).
22. Green, M. S. Markoff random processes and the statistical mechanics of time-dependent phenomena. II. Irreversible processes in fluids. *J. Chem. Phys.* **22**, 398–413 (1954).

23. Kubo, R., Yokota, M. & Nakajima, S. Statistical-mechanical theory of irreversible processes. Response to thermal disturbance. *J. Phys. Soc. Jpn.* **12**, 1203–1211 (1957).
24. Hargus, C., Klymko, K., Epstein, J. M. & Mandadapu, K. K. Time reversal symmetry breaking and odd viscosity in active fluids: Green-kubo and nemd results. *J. Chem. Phys.* **152**, 201102 (2020).
25. Crocker, J. C. & Grier, D. G. Methods of digital video microscopy for colloidal studies. *J. Colloid Interf. Sci.* **179**, 298–310 (1996).
26. Bickel, T. A note on confined diffusion. *Phys. A* **377**, 24–32 (2007).
27. Metzler, R., Jeon, J.-H., Cherstvy, A. G. & Barkai, E. Anomalous diffusion models and their properties: non-stationarity, non-ergodicity, and ageing at the centenary of single particle tracking. *Phys. Chem. Chem. Phys.* **16**, 24128–24164 (2014).
28. Nourhani, A., Ebbens, S. J., Gibbs, J. G. & Lammert, P. E. Spiral diffusion of rotating self-propellers with stochastic perturbation. *Phys. Rev. E* **94**, 030601 (2016).
29. Abate, A. R. & Durian, D. J. Approach to jamming in an air-fluidized granular bed. *Phys. Rev. E* **74**, 031308 (2006).
30. López-Castaño, M. A. et al. Pseudo-two-dimensional dynamics in a system of macroscopic rolling spheres. *Phys. Rev. E* **103**, 042903 (2021).
31. Lasanta, A., Vega Reyes, F., Prados, A. & Santos, A. When the hotter cools more quickly: Mpemba effect in granular fluids. *Phys. Rev. Lett.* **119**, 148001 (2017).
32. Rodríguez-Rivas, A., Romero-Enrique, J. M. & Rull, L. F. Molecular simulation study of the glass transition in a soft primitive model for ionic liquids. *Mol. Phys.* **117**, 3941 (2019).
33. Liu, R., Gong, J., Yang, M. & Chen, K. Local rotational jamming and multi-scale hyperuniformities in an active spinner system. Preprint at <https://arxiv.org/abs/2204.13391> (2022).
34. Codling, E. A., Plank, M. J. & Benhamou, S. Spiral diffusion of rotating self-propellers with stochastic perturbation. *J. R. Soc. Interface* **5**, 813 (2008).
35. Farhadi, S. et al. Dynamics and thermodynamics of air-driven active spinners. *Soft Matter* **14**, 5588–5594 (2018).
36. Workamp, M., Ramirez, G., Daniels, K. E. & Dijkstra, J. A. Symmetry-reversals in chiral active matter. *Soft Matter* **14**, 5572–5580 (2018).

Acknowledgements

We acknowledge funding from the Government of Spain through Agencia Estatal de Investigación (AEI) project No. PID2020-116567GB-C22). A.R.-R. also acknowledges financial support from Consejería de Transformación Económica, Industria, Conocimiento y Universidades de la Junta de Andalucía/FEDER for funding through project P20-00816 and FSE through post-doctoral grant no. DC00316 (PAIDI 2020). F.V.R. is supported by the Junta de Extremadura grant No. GR21091, partially funded by the ERDF. The authors are indebted to Prof. Ángel Garcimartín, for his important technical

and scientific assistance on the setting up of the laboratory where the experiments of this work were performed.

Author contributions

M.L.-C. designed the particles, performed all experiments, wrote most parts of the particle tracking code and prepared the first version of the manuscript. F.V.R. designed the air table set-up, conceived the experiments, assisted on the implementation of the particle tracking codes, wrote most parts of the post-particle-tracking codes for measurement and characterization of the particle dynamics. F.V.R. and A.R.-R. discussed the results, wrote the paper and co-directed the project.

Competing interests

The authors declare no competing interests.

Additional information

Supplementary information The online version contains supplementary material available at <https://doi.org/10.1038/s42005-022-01032-9>.

Correspondence and requests for materials should be addressed to Álvaro Rodríguez-Rivas.

Peer review information *Communications Physics* thanks Cory Hargus and the other, anonymous, reviewer(s) for their contribution to the peer review of this work.

Reprints and permission information is available at <http://www.nature.com/reprints>

Publisher's note Springer Nature remains neutral with regard to jurisdictional claims in published maps and institutional affiliations.



Open Access This article is licensed under a Creative Commons Attribution 4.0 International License, which permits use, sharing, adaptation, distribution and reproduction in any medium or format, as long as you give appropriate credit to the original author(s) and the source, provide a link to the Creative Commons license, and indicate if changes were made. The images or other third party material in this article are included in the article's Creative Commons license, unless indicated otherwise in a credit line to the material. If material is not included in the article's Creative Commons license and your intended use is not permitted by statutory regulation or exceeds the permitted use, you will need to obtain permission directly from the copyright holder. To view a copy of this license, visit <http://creativecommons.org/licenses/by/4.0/>.

© The Author(s) 2022